Journal of
Materials Chemistry A

Accepted Manuscript

This article can be cited before page numbers have been issued, to do this please use: Z. Su, C. Yang, C. Xu, H. Wu, Z. Zhang, T. Liu, C. Zhang, Q. Yang, F. Kang and B. Li, *J. Mater. Chem. A*, 2013, DOI: 10.1039/C3TA13148C.

View Article Online
DOI: 10.1039/C3TA13148C

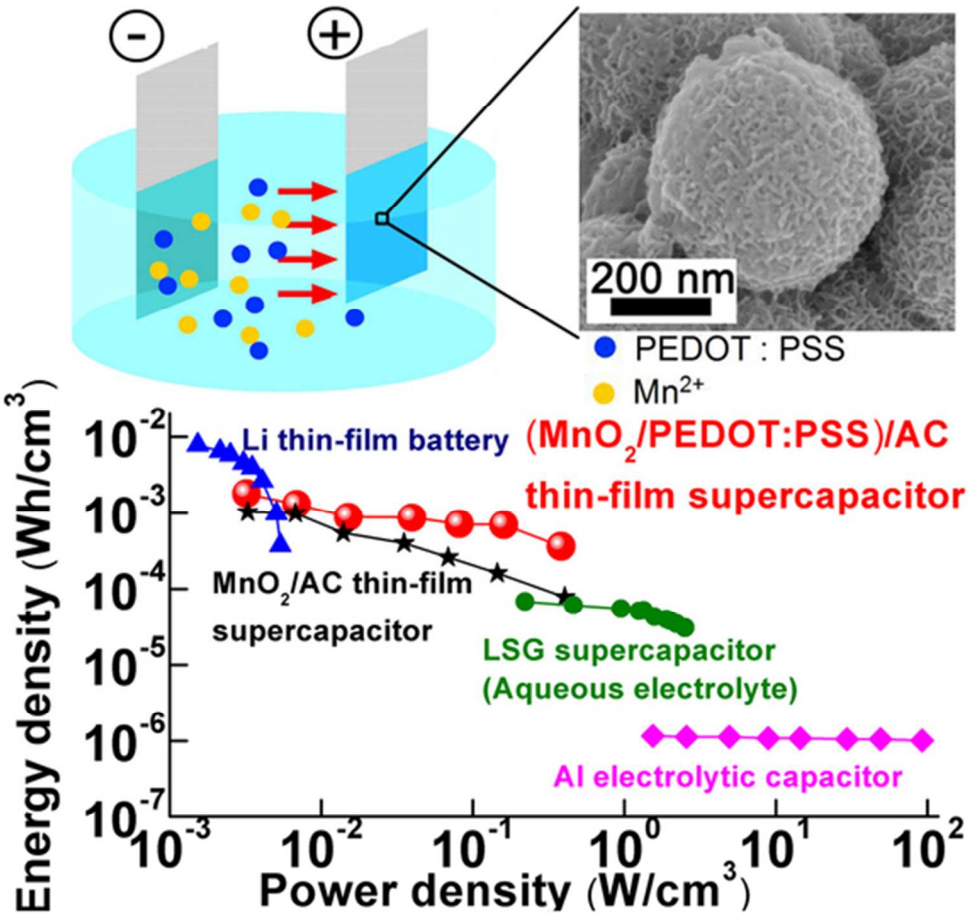

Using the co-electro-deposition strategy, MnO2/PEDOT:PSS electrode material with high areal capacitance (1670 mF/cm2 at 0.5 mA/cm2), high areal mass (8.5 mg/cm2) on a piece of ubiquitous stainless steel mesh current collector is obtained, which makes an aqueous assymetric supercapacitor with high energy density, power density and excellent rate capability.
49x45mm (300 x 300 DPI)

Cite this: DOI: 10.1039/c0xx00000x

www.rsc.org/xxxxxx

ARTICLE TYPE

Co-electro-deposition of the MnO_2/PEDOT:PSS Nanostructured Composite for High Areal Mass, Flexible Asymmetric Supercapacitor Devices

Zijin Su,[a] Cheng Yang,[a]* Chengjun Xu,[a] Haoyi Wu,[a] Zhexu Zhang,[a] Ting Liu,[a] Chen Zhang,[b] Quanhong Yang,[a,b] Baohua Li,[a] Feiyu Kang,[a,c]*

Received (in XXX, XXX) Xth XXXXXXXXX 20XX, Accepted Xth XXXXXXXXX 20XX
DOI: 10.1039/b000000x

To meet the rapidly growing demand, it's necessary to develop novel flexible energy storage devices with high energy density in limited area, fast charging ability, low cost for mass production, and miniaturized device size. To address the above issues, here we introduce the co-electro-deposition strategy, which is able to prepare the electrode material with high areal capacitance (1670 mF/cm^2 at 0.5 mA/cm^2), high areal mass (8.5 mg/cm^2),excellent mechanical robustness, high through-put and great convenience even on a piece of ubiquitous stainless steel mesh current collector. Based on this advancement, we are able to obtain an ultrathin (less than 200 μm) aqueous asymmetric supercapacitor device with high energy density (1.8×10^{-3} Wh/cm^3), high power density (0.38 W/cm^3 at 3.62×10^{-4} Wh/cm^3) and excellent rate capability. This energy storage device is integrated into a prototype smart card to drive a light emitting diode (LED) indicator, which is charged for 5 seconds and can light up the indicator for more than 2 hours, demonstrating great promise in miniaturized novel flexible energy storage devices.

1. Introduction

For the blooming wearable and rolling-up consumer electronics, e.g. electronic papers, collapsible displays, and flexible tablet PCs *etc.*, the bulky battery packs are no longer applicable since they are rigid giant components which occupy a large volume of the total device. To address this issue, materials scientists and engineers have been conducting researches in the design and fabrication of novel miniaturized power sources with superior electrochemical properties and many others, *e.g.* lightweight, flexibility, high mechanical integrity upon bending and rolling, and the fast charging character.[1, 2] Recently, significant advances have been made in this area. For example, El-Kady *et al.* have fabricated high-power graphene micro-supercapacitors for flexible energy storage,[3] Jung *et al* have used carbon films to make transparent, flexible supercapacitor.[4] Also, some novel, flexible and high-performance batteries have been made.[5-8]

Supercapacitors (or ultracapacitors, electrochemical capacitors) exhibit a series of advantagesas compared with batteries, such as high power density, long cycle life, fast charging-discharging rate within seconds, can be totally made of non-toxic materials, do not combust when punctured, and high reliability.[9, 10] Moreover, supercapacitors can be fabricated into thin and small configurations in more simple processing methods and can be paired with energy conversion devices such as thermoelectrics, solar panels and piezoelectrics to build up self-powered devices.[11] Yet they are facing a few challenges *e.g.* low working voltage and low energy density.

In order to improve the electrode capacitance, pseudocapacitive materials are being investigated, such as RuO_2,MnO_2,[12, 13] NiOand Co_3O_4*etc*. Among the transition-metal oxides, MnO_2 is generally considered to be one of the most promising candidates because of its high theoretical specific capacitance (as high as 1370 Fg^{-1}), low cost, environmental friendliness and nature abundance.[10, 14] However, the poor electrical conductivity of MnO_2 (10^{-5} - 10^{-6} S/cm) results in low gravimetric capacitance (50 - 250 F/g) and thus hinders the wide application in energy storage systems.[14-17] An effective strategy is to combine MnO_2 with conductive materials such as carbon nanotube (CNT), graphene, and carbon nanofiber (CNF) *etc*.,[12, 18-20]and intrinsic conductive polymers *e.g.*polypyrrole (PPy), poly(3,4-ethylenedioxythiophene) (PEDOT),[21] poly(3,4-ethylenedioxythiophene):poly(styrene sulfonate) (PEDOT:PSS) [12, 22] and polyanilline (PANI).For example, our group recently studied the combination of MnO_2 with PANI to improve the electrochemical performance;[23]some other groups investigated the wrappage of the MnO_2-graphene nanostructures with the conductive polymers.[24]Benefit from this materials combination, a higher specific capacitance with a higher MnO_2 loading content can be achieved when compared to the traditional carbon based composites. However, due to the limited mixing efficiency, a large amount of conductive materials (*e.g.* carbon and conductive polymers) are necessary in the metal oxide composite, and thus the capacitance of the electrode is compromised.[25] On the other hand, binder materials such as polytetrafluoroethylene (PTFE) are needed to improve the mechanical strength and cohesiveness, since it has no contribution to either conductivity and capacitance, the electrode performance is further inhibited.[10]Besides, for preparing the thin film electrodes, conventional dispensing and

View Article Online
DOI: 10.1039/C3TA13148C

printing methods for the electrode materials suffer from the weak contact at the interface and often result in mechanical failure upon bending.

Considering the disadvantages of conventional combinationmethods,[12]the development of novel electrode preparation methods becomes urgently necessary. In comparison, electrodeposition and electrophoretic deposition (EPD) methods are more advantageous since they are both scalable and inexpensive techniques in industrial process which can result in very uniform films.[26, 27] Yet they are comparatively time consuming to obtain thick films of the active mass based on these methods due to the weak electrical conductivity of metal oxides;[8] for example, in a most recent report, it takes more than 1400 minutes (about one day) to electrodeposite 10 mg/cm^2 of MnO_2 on the substrates,[26] which is impractical in preparing composite electrodes with a high mass loading, which is critical to the areal capacitance of the supercapacitor. Considering the fact that within the same area of footprint, the electrode which high areal capacitance can store more charges; this character is crucial in miniaturization of the energy storage device for the gadget applications.[28]

Herein we first report the co-electro-deposition of the uniform MnO_2/PEDOT:PSS nanostructured composite electrode for supercapacitor. This scheme does provide a large areal capacitance (1670 mF/cm^2). Even though the areal capacitance is not the highest compared with some 3D structured electrodes,[29, 30] it is much higher than most supercapacitor based on metal substrate.[31-33] Different from any published report, this manuscript discloses an effective method, using a cheap and common composite, i.e. MnO_2/PEDOT:PSS to demonstrate the new idea, that high areal capacitance up to 1670mF/cm^2 can be achieved even on low specific area substrates. The scheme also shows a scalable process to obtain thicker films of the active mass (over 8 mg/cm^2 within 20 minutes). Moreover, this concept does not conflict with those methods which achieving high areal capacitance due to using 3D porous substrates. We select asymmetric supercapacitor structure as the motif for study, which renders higher working potential and higher power density. Briefly, MnO_2 and a small dose of PEDOT:PSS are simutaneouslydeposited onto a piece metal current collector (stainless steel mesh) in an aqueous stock solution containing both PEDOT:PSS and Mn^{2+}. PEDOT:PSS acts as both the conductive additive and the polymer binder, and it is uniformly combined with MnO_2 during the anode deposition process of Mn^{2+}. The deposition of PEDOT:PSS, on the other hand, is driven by EPD, which is a physical process instead. We found that even though PEDOT:PSS is as less as 9.9 wt% in the composite (in another word, over 90 wt% of the electrode material is MnO_2), it effectively controls the thickness of the composite film and drastically improves both the electrochemical property as well as mechanical robustness. For the current collector material, we adopt the commercial stainless steel mesh substrate (64 μm in thickness) due to its stable superficial area, low cost, strong impact resistance, superior chemical stability and high electrical conductivity. With the above basic design, the as-prepared composite is robust enough to resist the peeling force without the addition of any binder and exhibits excellent electrochemical performance and is featured with a very low cost. In the following paragraphs, we'd like to give a detailed elucidation of this new material and demonstrate its application in fabricating a ultrathin asymmetric supercapacitor which can drive a prototype smart card.

2. Experimental

2.1 Preparation of MnO_2/PEDOT:PSS Nanostructured Composite Electrode

The MnO_2/PEDOT:PSS composite was synthesized by anode deposition and EPD on a piece of stainless steel wire mesh. Prior to deposition, the stainless steel wire mesh was washed by ultrasonication in a mixed solution of acetone and ethanol (1:1 vol). Rectangular-shaped electrodes (1.5 × 2.0 cm^2, thickness ~ 64 μm) were used. Metal mesh was used as anode and the counter electrode was Pt plate. The co-electro-deposition process was performed in an aqueous solution containing 80 mL (0.1 M) of manganese (II) acetate and 0.4 mL PEDOT:PSS aqueous solution (1 wt %) with a 10.0 V DC voltage. Since the content of both Mn^{2+} and PEDOT:PSS are in great excess as compared with the deposited composite mass, it can be regarded that the concentration of the solution is constant. The control sample of the pure MnO_2 deposited electrode was prepared in a 0.1 M manganese acetate aqueous solution (80 mL). The obtained electrodes were rinsed with deionized water for several times to remove the impurities and dried at 60 ℃ for 1 h.

2.2 The Fabrication of Asymmetric Aqueous Supercapacitor

The activated carbon electrode was prepared by mixing 80% activated carbon, 10% acetylene black and 10% PVDF. The mixture was casted onto PET orAl foil as negative electrode. This electrode was pressed and combined with MnO_2/PEDOT:PSS electrode with 0.5 M Na_2SO_4 as electrolyte and a separator (NKK TF44 25μm) in between. The mass loading of MnO_2/PEDOT:PSS and activated carbon are 0.94 mg/cm^2 and 0.99 mg/cm^2, respectively. The supercapacitor was packaged by PET films and EVA hot melt glue.

2.3 Materials Characterization and Electrochemical Measurements

The morphology and microstructure of the composites were characterized by field emission scanning electron microscopy (FE-SEM, HITACH S4800, Japan) and transmission electron microscopy (TEM, JEOL-2100F). X-ray photoelectron spectroscopy (XPS) measurements (ESCALAB 250Xi) were performed to analyze the surface species and their chemical states. Deconvolution and spectral line fitting were carried out using XPS Peak 4.0. Raman spectra were recorded on a Jobin-Yvon Horbia 800 using a 632.8 nm laser. The Zeta potential of PEDOT: PSS was determined with a zetasizer (Malvern Zetasize Nano ZS, Malvern Instruments).

The electrochemical properties of the as-prepared samples were investigated on an electrochemical station (VMP3, Bio-Logic, France) by a typical three-electrode configuration in a Na_2SO_4 (0.5 M) aqueous electrolyte. The working electrodes were the as-prepared samples with an electrode area of 3 cm^2, platinum and saturated calomel electrode (SCE) were used as counter and reference electrodes, respectively. The applied potential window of cyclic voltammetry and galvanostatic charging/discharging was in the range from 0.0 V to 1.0 V. The electrochemical impedance spectroscopy (EIS) was conducted in the frequency range between 100 KHz and 0.01 Hz. The specific capacitance was calculated from the CVs and discharging curves according to the equations:

$$C = \frac{1}{m \cdot v \cdot \Delta V} \int i(V) dV \quad (1)$$

$$C = \frac{I \cdot \Delta t}{m \Delta U} \quad (2)$$

View Article Online
DOI: 10.1039/C3TA13148C

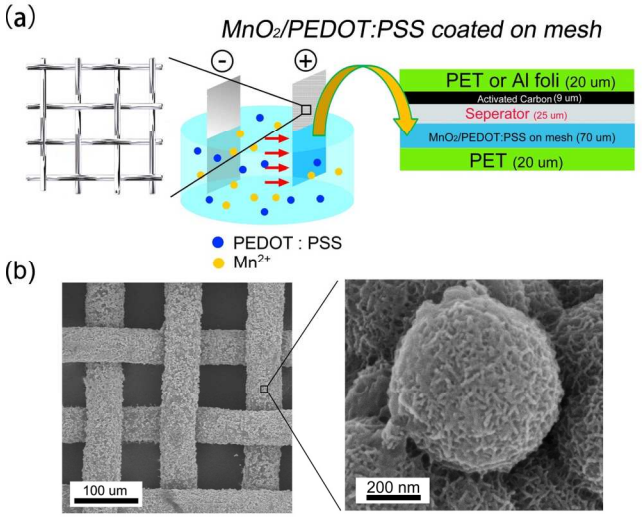

Fig 1. (a) Schematic of the fabrication process: the MnO_2/PEDOT:PSS nanocomposite is co-electro-deposited onto the stainless steel mesh (anode) and then it is fabricated in the asymmetrical supercapacitor as the positive electrode and activated carbon as negative electrode. (b) SEM images of the MnO_2/PEDOT:PSS nanocomposite at low and high magnifications.

where, C is the specific capacitance of materials, m is the mass loading on the substrate, v is the scan rate, ΔV is the potential window in the CV curves, $i(V)$ is the voltammetric current, I is the applied current density, ΔU is potential window in discharging process and Δt is the discharging time.[23] The energy and power density (E and P) were calculated by the equation:

$$E = (\int IV(t)dt / (Vol) \qquad (3)$$

$$P = E / \Delta t \qquad (4)$$

where I is the discharging current, $V(t)$ is the discharging current excluding the IR drop, dt is the time differential, Δt is the discharging time and Vol refers to the volume of the device, respectively. It is worth mentioning that the volumetric capacitance includes active material, the substrate (or the current collector) and the separator with electrolyte.

3. Results and Discussion

In our design, EPD is selected to deposit PEDOT:PSS, while MnO_2 is deposited through the anode deposition. EPD has attracted increasing attention both in academia and industrial sectors not because its highly versatile applications but also because of the cost-effectiveness and the requirement of simple apparatus.[34] Other advantages of EPD include strong adherence, high density and excellent homogeneity of the coating.[6] In the stock solution containing both PEDOT:PSS and Mn^{2+}, PEDOT: PSS (Zeta potential is -24.65 mV at pH = 3.45) was driven by the electrostatic field and was tightly attached to the in-situ formed MnO_2 at the anode surface, forming a nanostructured composite film. The resulting composite showed high specific capacitance (503 F/g at 1 mV/s in 0.5 M Na_2SO_4) and excellent electrochemical cyclability (99.5% specific capacitance retention after 4000 cycles). Using this method, thick electrode films can be conveniently obtained, since the presence of PEDOT:PSS facilitates the charge transfer process for Mn^{2+} at the electrode surface. By elongating the time of electric field applied, a high mass loading of the MnO_2/PEDOT:PSS (8.4 mg/cm^2) composite is conveniently prepared, which exhibits excellent areal capacitance (1.67 F/cm^2 at 0.5 mA/cm^2). To further demonstrate the potential of the hybrid electrode for ultrathin and light-weight applications, we fabricated a 1.5×4 cm^2 2.0 V asymmetric supercapacitor assembled with the MnO_2/PEDOT:PSS positive electrode and activated carbon film negative electrode. This supercapacitor device shows a maximum volume energy density and power density of ~1.80×10^{-3} Wh/cm^3 and ~0.38 W/cm^3 respectively. What's more, it shows excellent rate capability with a good rectangular CV curve even at the scan rate of 2.0 V/s.

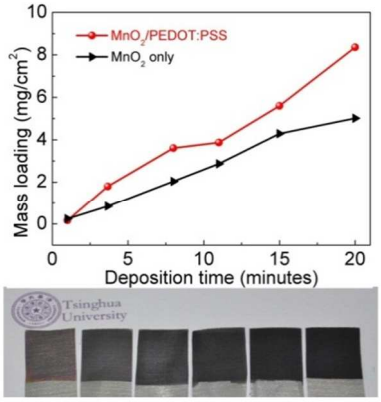

Fig. 2 Up: A plot showing the mass loading *vs.* deposition time of MnO_2/PEDOT:PSS and control MnO_2. Down: The corresponding MnO_2/PEDOT:PSS nanocomposite deposited on stainless steel substrate with different mass loadings. (The mass increases from left to right).

Fig. 1a briefly illustrates the electrode and supercapacitor fabrication process. MnO_2/PEDOT:PSS nanocomposite was conformally deposited on the surface of the stainless steel substrate using co-electro-deposition. This electrode is used as the positive electrode and activated carbon (AC) film is used as the negative electrode. Thus the supercapacitor is an asymmetric one. The as-prepared supercapacitor device is ultrathin, flexible and light-weight.

The one-step co-electro-deposition method we used involves two techniques: anode deposition and EPD. The electrochemical preparation of manganese oxide from an aqueous solution of Mn^{2+} has been widely reported. The electrochemical reaction of the manganese oxide formation can be described as follows:

$$Mn^{2+} + 2H_2O \rightarrow MnO_2 + 4H^+ + 2e^- \qquad (5)$$

On the other hand, EPD was carried out for the PEDOT: PSS deposition. In our experiment, the Zeta potential of the PEDOT:PSS aqueous solution was recorded to be -24.65 mV at pH = 3.45. The attachment of PEDOT:PSS on the electrodes can be simply attributed to the Coulomb force driven by the electric field.

View Article Online
DOI: 10.1039/C3TA13148C

Fig. 1b shows the photographic image of the stainless steel meshes after the MnO_2/PEDOT:PSS deposition. As can be seen in **Fig. 2**, the surface becomes darker as the deposition time increases, which indicates that MnO_2/PEDOT:PSS is effectively deposited on the surface. The MnO_2 and MnO_2/PEDOT:PSS mass contents increase with the deposition time almost linearly and the deposited mass of MnO_2/PEDOT:PSS is about twice of that of MnO_2 under the same deposition time and electric field, which is due to the improved electrical conductivity with the present of PEDOT:PSS. In this method, we can easily obtain high mass loadings of the active materials as high as 8.4 mg/cm^2

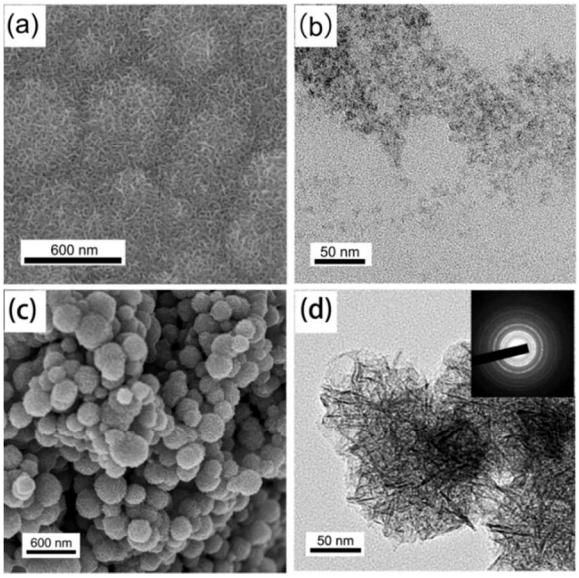

Fig. 3 (a) SEM and (b) TEM images of the anode-deposited pure MnO_2 electrode material. (c) SEM and (d) TEM images of the co-electro-deposited MnO_2/PEDOT:PSS electrode material. The inset in (d) is the selected area electron diffraction pattern of the same sample.

within 20 minutes on the stainless steel substrate with the applied voltage of 10.0 V. As compared to some recently reported techniques for fabricating the composite electrode materials, this is much effective, e.g., it is 20 times faster than Hu's report in preparing MnO_2/conducting material composite electrode and 60 times faster than Sumboja's report in preparing MnO_2/graphene sheet composite electrode.[28, 35] It reveals that this is a highly efficient method to prepare supercapacitor electrodes as compared to the other available deposition methods.[36, 37]

In order to evaluate the adhesion strength and cohesiveness of the MnO_2/PEDOT:PSS nanocomposite active mass on the stainless steel current collector,we attached a piece of scotch tape to the dried MnO_2 and MnO_2/PEDOT:PSS film with a full contact.[6]Then it was peeled off by hand and the surfaces on both sides were carefully observed to evaluate the adhesion property of the active mass towards the current collector. Experimental result suggests that the MnO_2/PEDOT:PSS composite film is robust enough to resist the peeling force, while the control sample (the film with the control pure MnO_2) was easily peeled off by the tape. As **Fig. S2** shows, when the scotch tape was removed, some black powders from the pure MnO_2 film were transferred to the tape, and the underlying metal parts of the stainless steel current collector was exposed. The MnO_2/PEDOT:PSS film, however, exhibited un-noticeable detachment from the mesh, even by peeling for several times, when the film was warped by repeatedly peeling. The reason of adhesion enhancement is that the interaction between MnO_2 and the substrate is dominated by van der Waals force. However the mechanical property of MnO_2 is poor and the van der Waals force to the substrate is weak. Compared with pure MnO_2, MnO_2 and PEDOT:PSS are uniformed combined with each other during the co-electro-deposition process, and thus PEDOT:PSS acts as the polymer binder which significantly enhances the integrity of the composite. Additionally, PEDOT:PSS to some extent has better contact with the metal mesh substrate and gives mechanical interlocking effect besides van der Waals force.This experiment as shown in **Fig. S2** indicates that PEDOT:PSS is able to function as an excellent binder for the MnO_2 electrode.

Fig. 3 a and c shows the over-view images of scanning electron microscopy (SEM) of the MnO_2 and MnO_2/PEDOT:PSS samples, respectively. The MnO_2 without PEDOT:PSS appears to have a smooth surface on the stainless steel mesh. However, the top layer of the MnO_2/PEDOT:PSS appears to be uniform assemblies of nanospheres with rough surface textures (**Fig. S3a**). The diameter of the nanospheres ranges from 100 nm to 500 nm. This morphology is analogous to the prior reports regarding the MnO_2 nanostructures obtained from the redox preparation method.[36]

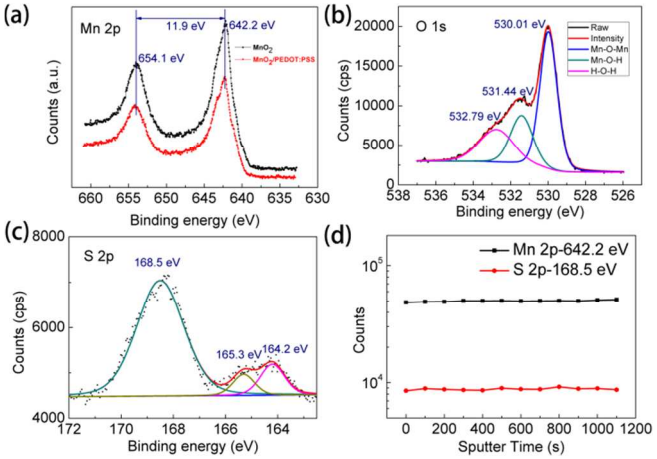

Fig. 4 (a) Mn 2p, (b) O 1s, , (c) S 2p core level XPS spectrum of the MnO_2/PEDOT:PSS nanocomposite. (d) XPS depth-profile of the same sample. It shows that the ratio between element Mn and S is constant with the sputtering time.

From the SEM images and the corresponding EDAX (**Fig. S4**) analysis, we can find that PEDOT: PSS was entangled with MnO_2 and there is no distinct boundary between MnO_2 and PEDOT:PSS. MnO_2 and MnO_2/PEDOT:PSS samples were scratched from the meshes for TEM tests. **Fig. 3b** shows that the control MnO_2 sample obtained through the anode deposition process is only composed of scattered powders, indicating the low cohesiveness of the material. As compared, the MnO_2/PEDOT:PSS nanocomposite still keeps the assembly of spherical nanoparticles which suggests that the addition of PEDOT:PSS improves the cohesiveness between the MnO_2, and both PEDOT:PSS and MnO_2 are combine well with each other. This is further confirmed by the high resolution TEM analysis, as shown in **Fig. S3b**, which gives a clearer view of the nanocomposite. Selected area electron diffraction (SAED) from the same area is shown in the inset of **Fig. 3d**, showing that the deposited MnO_2 are crystalline.

X-ray photoelectron spectroscopy (XPS) spectra of the MnO_2/PEDOT:PSS electrodes were used to determine the oxidation state of the as-prepared MnO_2. The XPS full spectrum (**Fig. S5a**) containing signals from Mn, O, S and C elements indicates the presence of both MnO_2 and PEDOT:PSS. Mn 2p spectra (**Fig. 4a**) show that Mn $2p_{3/2}$ and Mn $2p_{1/2}$ of both pure MnO_2 and MnO_2/PEDOT:PSS electrode materials have the

View Article Online
DOI: 10.1039/C3TA13148C

binding energy centering at 642.2 eV and 654.1eV respectively, with an energy separation of 11.9 eV, which is in good agreement with the reported data for MnO_2.[38, 39] It also indicates that the introduction of PEDOT:PSS didn't change the oxidation state of MnO_2. The separation of peak energies (ΔE_b) between the two peaks of Mn 3s components can be used as an indicator of Mn oxidation state in manganese oxides. **Fig. S5b** shows that the ΔE_b is 4.98eV between 4.8 and 5.3 eV, which is the peak separation of Mn^{4+} and Mn^{3+}, respectively.[23, 39] It suggests an intermediate oxidation state between Mn^{4+} and Mn^{3+}. An reported method is used to calculate the average valence of Mn by analysis of O 1s spectra (**Fig. 4b**).[39] The average Mn valence in MnO_2 is estimated to be 3.64 eV, coinciding with the analysis of Mn 3s spectrum. The XPS spectra of sulfur 2p for the MnO_2/PEDOT:PSS composite are shown in **Fig. 4c**. The peaks at 164.2 eV and 165.3 eV correspond to the sulfur atom of PEDOT. The higher binding

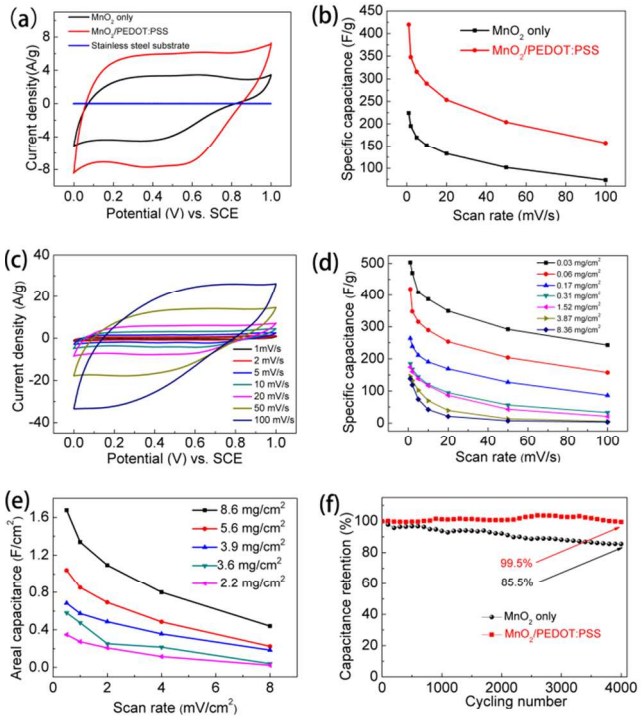

Fig. 5 (a) CV curves of stainless steel mesh substrate, MnO_2 and MnO_2/PEDOT:PSS at 20 mV/s. (b) Comparison of the specific capacitance between MnO_2 and MnO_2/PEDOT:PSS versus scan rate. (c) CV curves of MnO_2/PEDOT:PSS electrodes at different scan rates. (d) Specific capacitance *vs.* scan rate of the MnO_2/PEDOT:PSS electrodes with different mass loading. (e) Areal capacitance *vs.* scan rate for electrodes with different mass loading. (f) Comparison of cycling properties for MnO_2 and MnO_2/PEDOT:PSS electrodes up to 4000 cycles at 50 mV/s.

energy peak at 168.5 eV corresponds to the sulfur atom from PSS.[40, 41] XPS depth-profile is performed to determine the variations of the concentration of Mn and S element in the MnO_2/PEDOT:PSS film. **Fig. 4d** shows that with the increase of sputter time (0~1100 seconds), the signal intensity of Mn 2p and S 2p are almost constant, which confirms that the co-electro-deposition process can result in a uniform combination of MnO_2 and PEDOT:PSS in nanoscale.

Electrochemical performance of the samples of MnO_2 and MnO_2/PEDOT:PSS was measured. **Fig. 5a** shows the CV curves of stainless steel substrate, MnO_2 and MnO_2/PEDOT:PSS at the scan rate of 20 mV/s. The line-like CV curve of stainless steel substrate suggests that the substrate hardly contribute to the capacitance of the electrode. The CV curve of MnO_2/PEDOT:PSS shows better rectangular shape and larger area than MnO_2. It indicates that MnO_2/PEDOT:PSS has better capacitive behavior. **Fig. 5c** shows the CV curves of MnO_2/PEDOT:PSS at different scan rate ranging from 1 to 100 mVs^{-1}. The dependence of MnO_2/PEDOT:PSS specific capacitance versus scan rate is plotted in **Fig. 5b**, suggesting a larger specific capacitance than the pure MnO_2. (The specific capacitance is calculated by Eq. (1))The capacitance is lower at high scan rates because the electrolyte ions are difficult to fully access the interior surfaces of active materials due to the reduced diffusion time. [23]

As far as we know, thinner active material layer and slower scan rate lead to better specific capacitance performance of a supercapacitor, which is related to the transport efficiency of both electrons and ions during the electrochemical process. Yet in practical applications, high loading density of the active mass and high scan rate property are both necessary. Moreover, from the device aspect, the power performance of the supercapacitor depends on the total mass of the supercapacitor, including electrolyte, electrodes, separator and current collectors, *etc*.[37] Therefore, we investigated the relationship between mass loading and scan rate, so as to optimize the proper mass loading of active materials for different devices by this method. **Fig. S6** shows the CV scans of MnO_2/PEDOT:PSS with different mass loading at 20 mV/s. The CV shapes remain nearly rectangular at low mass loadings; however, with the mass loading increases the CV shapes show more deviations. The specific capacitances with respect to the mass of MnO_2/PEDOT:PSS are plotted in **Fig. 5d**. A specific capacitance of 503 F/g can be achieved at 1 mV/s. The specific capacitance decreases with the mass loading and increases with the scan rate. The specific capacitance decreases dramatically with the increase of scan rate at low scan rates, and remain nearly constant when the scan rate is higher than 20 mV/s. It has been revealed that as the mass loading increases, the specific capacitance decreases due to the kinetics of ion transports in electrodes with low ion diffusion constants.[37] **Fig. 5e** demonstrates the areal capacitance versus different MnO_2/PEDOT:PSS electrode mass loadings. A high areal capacitance has been achieved up to 1670 mF/cm^2 at the current density of 0.5 mA/cm^2, which is advantageous over the previously reported results on areal capacitance.[25, 28, 35] Considering the fact that with the mass loading increases, the areal capacitance increases accordingly. Therefore, by increasing the mass loading, a higher areal capacitance can be obtained easily by this method.

Cycle life is an important parameter for the supercapacitor. The cycle life experiment over 4000 cycles for the MnO_2 and MnO_2/PEDOT:PSS composite was carried out at 50 mV/s. Unlike many other reported metal oxide/conductive polymer composites which have a poor cycle life, **Fig. 5f** demonstrates an excellent cycling performance of this composite. We found that the capacitance retention was 99.5% after 4000 cycles compared with 85.5% retention of capacitance after 4000 cycles of the control pure MnO_2 electrode. The excellent cycling performance of MnO_2/PEDOT:PSS electrode is also evidenced by the almost overlapped CV curves of the first and the 4000th cycle, as shown in **Fig. S7**. The results suggest that the small amount of PEDOT:PSS (9.9% by weight in the composite which is calculated by the data from Tab. S1) acts as an excellent binder for the nanocomposite.

View Article Online
DOI: 10.1039/C3TA13148C

To demonstrate the viability of forming a device, an aqueous asymmetric supercapacitor was fabricated instead of symmetric supercapacitor. The asymmetric supercapacitor has higher working voltage compared with symmetricone which has a voltage about 1.0 V. And it is more suitable for real portable electronics such as driving LED and mini-speaker, a higher voltage e.g. 3 V is a must. The asymmetric supercapacitor was fabricatedusing MnO_2/PEDOT:PSS as the positive and activated carbon as the negative electrodes, respectively. In order to evaluate the electrochemical properties and estimate the stable potential windows of the MnO_2/PEDOT:PSS composite and activated carbon, CV measurements were performed on the two electrode materials in the 0.5 M Na_2SO_4 electrolyte before the test of a full cell. A three electrode system with a platinum foil as counter electrode and a saturated calomel electrode (SCE) as reference electrode was used. The MnO_2/PEDOT:PSS was measured within a potential window of 0 ~ 1.0 V, while activated carbon was measured within a potential windonw of -1.0 ~ 0.2 V at scan rate of 20 mV/s, as shown in **Fig. 6a**. The CV curves indicate that the voltage of the asymmetric supercapacitor can be as high as 2.0 V. To further demonstrate the large voltage window of the supercapacitor, CV measurements were carried out with different voltage windows at 20 mV/s (**Fig. 6b**). The aqueous supercapacitor demonstrates an ideal capacitive behavior with rectangular CV curves, even at the potential window as large as 2.0 V.

To evaluate the electrochemical properties of the asymmetric supercapacitor, we carried out the CV measurements at different scan rates ranging from 10 to 100 mV/s. The device shows an excellent rectangular CV geometry, indicating a better capacitive behavior. Surprisingly, the CV curve still remains a good rectangular shape even when a high scan rate (2.0 V/s) is applied (**Fig. S8**). This demonstrates a good rate capability of the full cell.For further understanding, the electrochemical impedance spectroscopy (EIS) of MnO_2/AC and (MnO_2/PEDOT:PSS)/AC asymmetric supercapacitors was measured in the frequency range of 100 kHz ~ 10 MHz at open circuit potential with an ac perturbation of 5 mV (**Fig. 6d**). The measured impedance spectra were analyzed using complex nonlinear least-squares (CNLS) fitting method.[42] The electrical equivalent circuit was given in **Fig. S9**. At high frequency, the intercept at real part represents a combined resistance of ionic resistance of electrolyte, intrinsic resistance of substrate and contact resistance at the active material/current collector interface (*R*e),[43] and *R*ct refers to the charge-transfer resistance caused by the Faradic reactions and the double-layer capacitance on the grain surface.[44]According to the impedance spectra, the *R*e/*R*ct of (MnO_2/PEDOT:PSS)/AC supercapacitor is 0.48 Ω/9.50 Ω compared with 0.65 Ω/11.76 Ω of the control MnO_2/AC supercapacitor. The *R*e value is almost the same for both supercpapacitors. However, the *R*ct of (MnO_2/PEDOT:PS)/AC supercapacitor is lower than the MnO_2/AC supercapacitor as a result of the conductivity enhancement of MnO_2/PEDOT:PSS composite. The good capacitive behavior and low internal resistance were further confirmed by the Galvanostatic charge-discharge experiment of the (MnO_2/PEDOT:PSS)/AC supercapacitor device. **Fig. 6e** shows the nearly triangular shape of the charging-discharging curves at current density of 50 mA/cm^3, indicating the fast ion transport within the electrodes.[45] Furthermore, these charge-discharge curves show only a small voltage drop of 0.029 V at the start of the discharge curve, indicating a device with a low internal resistance. Discharge curves of supercapacitor devices at various current densities were shown in **Fig. 6f** and **Fig. S10**.

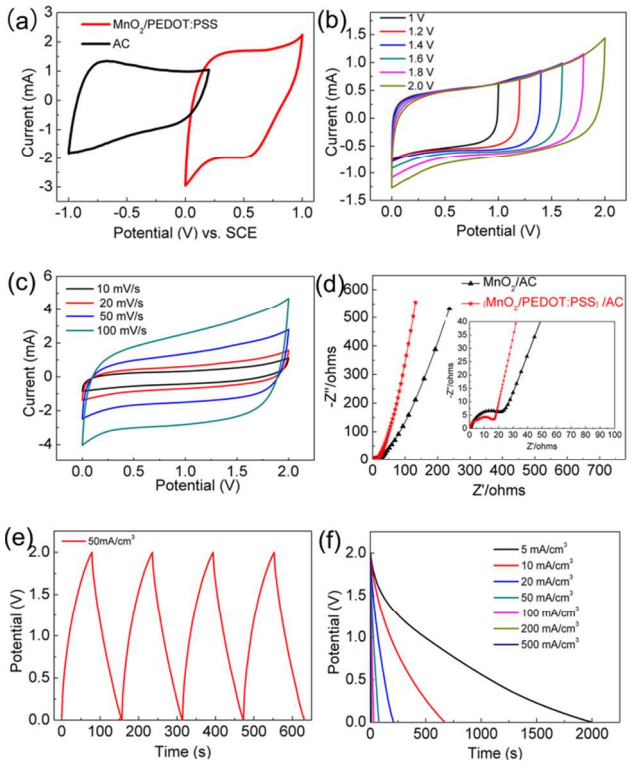

Fig. 6 (a) Comparative CV curves of MnO_2/PEDOT:PSS and activated carbon electrodes performed in a three-electrode cell in 0.5 M Na_2SO_4 aqueous solution at the scan rate of 20 mV/s. (b) CV curves of an optimized (MnO_2/PEDOT:PSS)/AC supercapacitor measured at different potential windows in 0.5M Na_2SO_4 aqueous solution at a scan rate of 20 mV/s. (c) CV curves of (MnO_2/PEDOT:PSS)/AC supercapacitor at the scan rates of 10, 20, 50, 100 mV/s. (d) Nyquist plots of the EIS for aqueous supercapacitor. (e) Galvanostatic charge/discharge curves obtained at current density of 50 mA/cm^3. (f) Discharging curves of the (MnO_2/PEDOT:PSS)/AC asymmetric supercapacitor at different current density from 5 to 500 mA/cm^3.

Fig. 7a shows a Ragone plot of the fully assembled supercapacitor devices reported in this manuscript and some other recently reported ones for comparison. Considering the fact that these devices are specially designed for the thin film energy storage purposes, volumetric energy and power densities were used as the figure of merit; which were calculated based on the stack of the whole tested devices. The performance of the (MnO_2/PEDOT:PSS)/AC asymmetric supercapacitor was compared with MnO_2/AC supercapacitors, laser-scribed graphene-based (LSG) supercapacitors,[45] 3 V/30 μF aluminum electrolytic capacitors and a 500 μAh lithium thin-film battery.[45] It appears that our (MnO_2/PEDOT:PSS)/AC asymmetric supercapacitor device exihibits excellent energy and power densities. The energy density of (MnO_2/PEDOT:PS)/AC supercapacitor (as high as 1.80×10^{-3} Wh/cm^3) is higher than MnO_2/AC supercapacitor, which is twenty-five times higher than that of the aqueous LSG supercapacitor. What's more, the energy is three orders of magnitude lower than aluminum electrolytic capacitor. Even at a high power density of 0.38 W/cm^3, value that is about the seventy times higher than that of Li thin-film battery, the device still shows an energy density of 3.62×10^{-4} Wh/cm^3, approaching the lower end of Li thin-film battery.

As shown in **Fig. S11a** and **b**, the as-prepared supercapacitor exhibits excellent flexibility and it can even endure repeated twisting without any harm to its structural integrity. There is no apparent change on the CV curves under different bending angles

View Article Online
DOI: 10.1039/C3TA13148C

range from 0 to 120°(**Figure S11c**). It further confirms the excellent flexibility of the as-prepared supercapacitor. For demonstration of real application, the asymmetric supercapacitor was used to drive a red LED indicator (1.8 V, 20mA) (**Fig. S12**), and the size of the asymmetric supercapacitor was compared with a coin (US quarter dollar) and a piece of credit card, as shown in **Fig. S13**. To further evaluate the supercapacitor properties with the date reported, two supercapacitors were prepared in series and charged to 3.0 V to drive a red LED indicator. The LED indicator remained effective enough for indication for more than 2.5 hours, which is longer than the recently reported result by Zhou *et al*.[46]Moreover, the charging speed of such a single device to 2.0 V can be as fast as 13 s. As shown in **Fig. S14**, the self-discharge curve of the supercapacitor device obtained immediately after charging to 1.3 V is recorded. It appears that it takes 6.5 h to discharge from 1.3 V (V_{max}) to 0.65 V ($1/2V_{max}$) which indicatesmuch lower self-discharge property than some reported carbon based supercapacitor.[13, 47] Owning to the superior performance of our ultrathin supercapacitor, a prototype smart card with two inlay supercapacitors (connected in series) was prepared as shown in **Fig. 7b**. A piece of LED chip（1.8 V, 20mA）and a thin film switch were bonded on a piece of flexible circuit board and connected to the supercapacitors as well. Pressing the switch, the LED would light up, powered by the two supercapacitor in series (**Fig. 7b** and ESI Movie 1). Owning to the flexibility of supercapacitors, the smart card can be flexible and the bending angle is more than 60°. As **Fig. 7c** shows after charging for 5 seconds, the voltage of the power source in the smart card can reach as high as 2.6 V. The supercapacitor series can drive the red LED very bright for 40 minutes. The LED remained effective enough for indication after 2 hours.As shown in **Fig. S15a**, the smart card is as thin as 0.744 mm, even thinner than commercial credit card (0.8mm). The function of the smart card with inlay supercapacitor can be further supplemented by integrating other active components and modules such as organic light emitting diodes (OLEDs), sensors, actuators, speakers, and even wireless systems *et al*. Our ultrathin and rapid charging supercapacitor can be an excellent power driver for portable and miniaturized devices such a smart card. Meanwhile, by adjusting the fabrication parameters e.g. MnO_2/PEDOT:PSS mass loading, it's convenient to adjust the capacitance and other properties, and thus we do believe this is a promising method to produce high performance supercapacitor devices for various applications.

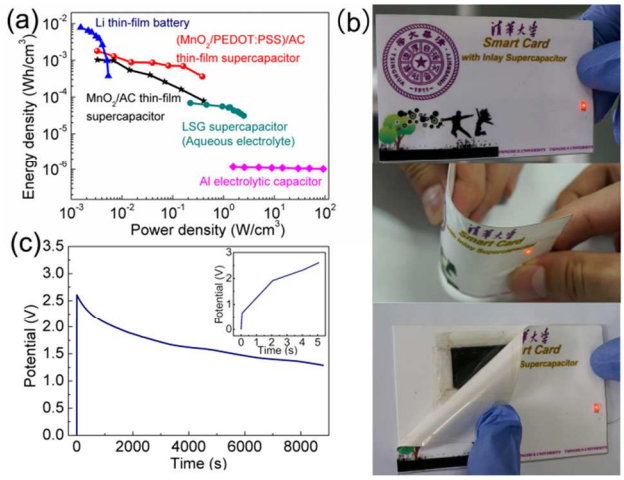

Fig. 7 (a) A Ragone plot showing the energy and power densities of (MnO_2/PEDOT:PSS)/AC supercapacitors compared with MnO_2/AC supercapacitors, LSG supercapacitors, aluminum electrolytic capacitors and a lithium thin-film battery.[45]The (MnO_2/PEDOT:PSS)/AC supercapacitors demonstrate high power and energy densities. (b) Photographs showing th a piece of prototyped smart card with two pieces of inlay asymmetric supercapacitors in series. A piece of LED indicator (1.8V, 20mA), a thin film switch, and a piece of flexible circuit board are assembled in the card, and the indicator is driven by the supercapacitors assmbled inside. Due to the high flexibility of as-fabricated supercapacitors the smart card can be flxible.(c) Charging and discharging curves of the supercapacitor series in the prototyped smart card. After charing for 5s the potential can be as high as 2.6V. The power source can drive red LED (1.8V, 20mA) very bright for 40 minutes and remain the LED effective after 2 hours. Inset in (c) shows the detail of the charging curve.

4. Conclusions

To sum up, we report a simple and highly efficient technology to fabricate the uniform MnO_2/PEDOT:PSS nanocomposite electrode in a one-step deposition process combined with both anode deposition and EPD. With this combination, we obtained a remarkably high performance nanocomposite electrode with thethickness up to 8.4 mg/cm^2 within 20 minuteseven on a ubiquitous substrate material i.e. stainless steel mesh. The as-obtained nanocomposite electrode contains over 90 wt% of MnO_2, which guarantees excellent capacitive property: the areal capacitance can reach as high as 1670mF/cm^2 at 0.5 mA/cm^2, which is advantageous over the previously reported results on areal capacitance of a single electrode for supercapacitor. Typically, this nanocomposite shows a maximum specific capacitance reaches 503 F/g at 1 mV/s, and shows 99.5% retention of specific capacitance after 4000 cycles at 50 mV/s. Asymmetric aqueous supercpapacitor based on such a MnO_2/PEDOT:PSS electrode shows high energy density (1.80×10^{-3} Wh/cm^3), power energy density (0.38 W/cm^3) and excellent rate capability, which is advantageous over many reported data regarding both energy density and power density.This method is very simple, efficient, and compatible to the industrial roll-to-roll process. The flexible, robust, ultrathin and high performance supercapacitor is a good candidate for the smart card inlay power source to realize much novel functionality. We believe this technology holds a promise for high-performance supercapacitor preparations and may find wide applications in the light-weight and ultrathin electronics. In addition, we envisage that when choosing high specific area substrate materials e.g. carbon nanofiber films, the areal capacitance of the electrode materials can be further boosted.

Acknowledgements:

This research is partially funded by the National Natural Science Foundation of China (51202120, 51232005), Shenzhen Government (JCYJ20120616215238779) and Guangdong Province Innovation R&D Team Plan (2009010025). The authors thanks Dr. Yanbing He and Dr. Yongye Liang for kind discussions and suggestions.

Notes and references:

[a] *Address, Division of Energy and Environment, Graduate School at Shenzhen, Tsinghua University, Shenzhen 518055, P. R. China. Fax: +86-755-26036417; Tel: +86-755-26036132; E-mail: yang.cheng@sz.tsinghua.edu.cn, fykang@sz.tsinghua.edu.cn*
[b] *Address, Key Laboratory for Green Chemical Technology of Ministry of Education, School of Chemical Engineering and Technology, Tianjin University, Tianjin, 300072, China*
[c] *State Key Laboratory of New Ceramics and Fine Processing, Department of Materials Science and Engineering, TsinghuaUniversity, Beijing 100084, China*

†Electronic Supplementary Information (ESI) available: [Analyses of SEM, TEM, XPS, Raman, electrochemicalproperty of the electrode

View Article Online
DOI: 10.1039/C3TA13148C

materials, and the details of fabrication of smart card prototype are elucidated. A movie showing the working process of smart card is also included.]. See DOI: 10.1039/b000000x/

1. B. G. Choi, J. Hong, W. H. Hong, P. T. Hammond and H. Park, *ACS Nano*, 2011, **5**, 7205.
2. F. Liu, S. Song, D. Xue and H. Zhang, *Adv Mater.*, 2012, **24**, 1089.
3. M. F. El-Kady and R. B. Kaner, *Nat. commun.*, 2013, **4**, 1475.
4. H. Y. Jung, M. B. Karimi, M. G. Hahm, P. M. Ajayan and Y. J. Jung, *Sci. Rep.*, 2012, **2**, 773.
5. N. Singh, C. Galande, A. Miranda, A. Mathkar, W. Gao, A. L. M. Reddy, A. Vlad and P. M. Ajayan, *Scientific Reports*, 2012, **2**, 481.
6. D. H. Ha, M. A. Islam and R. D. Robinson, *Nano Lett.*, 2012, **12**, 5122.
7. F. Liu, S. Song, D. Xue and H. Zhang, *Adv. Mater.*, 2012, **24**, 1089.
8. K. A. Jost, D. Stenger, C. R. Perez, J. McDonough, K. Lian, Y. Gogotsi and G. Dion, *Energy Environ. Sci.*, 2013, **DOI: 10.1039/C3EE40515J**
9. L. L. Zhang and X. S. Zhao, *Chem. Soc. Rev.*, 2009, **38**, 2520.
10. W. F. Wei, X. W. Cui, W. X. Chen and D. G. Ivey, *Chem. Soc. Rev.*, 2011, **40**, 1697.
11. T. Park, C. Park, B. Kim, H. Shina and Y. Kim, *Energy Environ. Sci.*, 2013, **6**, 788.
12. Y. Hou, Y. W. Cheng, T. Hobson and J. Liu, *Nano Lett.*, 2010, **10**, 2727.
13. D. Y. Zhai, B. H. Li, H. D. Du, G. Y. Gao, L. Gan, Y. B. He, Q. H. Yang and F. Y. Kang, *Carbon*, 2012, **50**, 5034.
14. G. H. Yu, L. B. Hu, N. A. Liu, H. L. Wang, M. Vosgueritchian, Y. Yang, Y. Cui and Z. A. Bao, *Nano Lett.*, 2011, **11**, 4438.
15. S. R. Sivakkumar, J. M. Ko, D. Y. Kim, B. C. Kim and G. G. Wallace, *Electrochim. Acta*, 2007, **52**, 7377.
16. R. Liu and S. B. Lee, *J. Am. Chem. Soc.*, 2008, **130**, 2942.
17. V. Subramanian, H. W. Zhu, R. Vajtai, P. M. Ajayan and B. Q. Wei, *J. Phys. Chem. B*, 2005, **109**, 20207.
18. S. Chen, J. W. Zhu, X. D. Wu, Q. F. Han and X. Wang, *ACS Nano*, 2010, **4**, 2822.
19. Z. S. Wu, W. C. Ren, D. W. Wang, F. Li, B. L. Liu and H. M. Cheng, *ACS Nano*, 2010, **4**, 5835.
20. J. G. Wang, Y. Yang, Z. H. Huang and F. Y. Kang, *Electrochim. Acta*, 2011, **56**, 9240.
21. R. Liu and S. B. Lee, *J. Am. Chem. Soc.*, 2008, **130**, 2942.
22. F. J. Liu, *J. Power Sources*, 2008, **182**, 383.
23. J. Wang, Y. Yang, Z. H. Huang and F. Kang, *J. Mater. Chem.*, 2012, **22**, 16943.
24. G. Yu, L. Hu, N. Liu, H. Wang, M. Vosgueritchian, Y. Yang, Y. Cui and Z. Bao, *Nano Lett.*, 2011, **11**, 4438.
25. A. E. Fischer, K. A. Pettigrew, D. R. Rolison, R. M. Stroud and J. W. Long, *Nano Lett.*, 2007, **7**, 281-286.
26. Y. He, W. Chen, X. Li, Z. Zhang, J. Fu, C. Zhao and E. Xie, *ACS Nano*, 2013, **7**, 174-182.
27. J. Bae, M. K. Song, Y. J. Park, J. M. Kim, M. Liu and Z. L. Wang, *Angew. Chem. Int. Ed.*, 2011, **50**, 1683.
28. A. Sumboja, C. Y. Foo, X. Wang and P. S. Lee, *Adv Mater.*, 2013, **25**, 2809.
29. T. Zhai, F. Wang, M. H. Yu, S. Xie, C. Liang, C. Li, F. Xiao, R. Tang, Q. Wu and X. H. Lu, *Nanoscale*, 2013.
30. J. R. McDonough, J. W. Choi, Y. Yang, F. La Mantia, Y. Zhang and Y. Cui, *Appl. Phys. Lett.*, 2009, **95**, 243109-243109-243103.
31. Y. Hou, Y. Cheng, T. Hobson and J. Liu, *Nano lett*, 2010, **10**, 2727-2733.
32. S. Sivakkumar, J. M. Ko, D. Y. Kim, B. Kim and G. Wallace, *ElectrochimActa*, 2007, **52**, 7377-7385.
33. H. Zhang, G. Cao, Z. Wang, Y. Yang, Z. Shi and Z. Gu, *Nano Lett*, 2008, **8**, 2664-2668.
34. L. Besra and M. Liu, *Prog. Mater. Sci.*, 2007, **52**, 1.
35. L. Hu, W. Chen, X. Xie, N. Liu, Y. Yang, H. Wu, Y. Yao, M. Pasta, H. N. Alshareef and Y. Cui, *ACS Nano*, 2011, **5**, 8904.
36. W. Chen, R. B. Rakhi, L. B. Hu, X. Xie, Y. Cui and H. N. Alshareef, *Nano Lett.*, 2011, **11**, 5165.
37. Q. A. Li, J. H. Liu, J. H. Zou, A. Chunder, Y. Q. Chen and L. Zhai, *J. Power Sources*, 2011, **196**, 565.
38. S. W. Lee, J. Kim, S. Chen, P. T. Hammond and Y. Shao-Horn, *ACS Nano*, 2010, **4**, 3889.
39. M. Toupin, T. Brousse and D. Belanger, *Chem. Mater.*, 2004, **16**, 3184.
40. J. Kim, J. Jung, D. Lee and J. Joo, *Synthetic Met.*, 2002, **126**, 311.
41. G. Greczynski, T. Kugler and W. Salaneck, *Thin Solid Films*, 1999, **354**, 129.
42. B. Conway, *Electrochemical supercapacitors: scientific fundamentals and technological applications (POD)*, Kluwer Academic/plenum. New York, 1999.
43. J. Gamby, P. Taberna, P. Simon, J. Fauvarque and M. Chesneau, *J. Power Sources*, 2001, **101**, 109.
44. Z. Fan, J. Yan, T. Wei, L. Zhi, G. Ning, T. Li and F. Wei, *Adv. Func. Mater.*, 2011, **21**, 2366.
45. M. F. El-Kady, V. Strong, S. Dubin and R. B. Kaner, *Science*, 2012, **335**, 1326.
46. C. Zhou, Y. Zhang, Y. Li and J. Liu, *Nano Lett.*, 2013, **13**, 2078.
47. J. R. McDonough, J. W. Choi, Y. Yang, F. L. Mantia, Y. Zhang and Y. Cui, *Appl. Phys. Lett.*, 2009, **95**, 243109-243109-243103.